

# Organic Electrochemical Transistor Aptasensor for Interleukin-6 Detection

Chiara Diacci, Bernhard Burtscher, Marcello Berto, Tero-Petri Ruoko, Samuel Lienemann, Pierpaolo Greco, Magnus Berggren, Marco Borsari, Daniel T. Simon,\* Carlo A. Bortolotti,\* and Fabio Biscarini



Cite This: *ACS Appl. Mater. Interfaces* 2024, 16, 61467–61474



Read Online

ACCESS |



Metrics & More



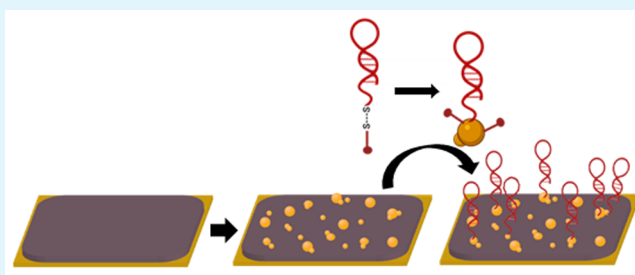
Article Recommendations



Supporting Information

**ABSTRACT:** We demonstrate an organic electrochemical transistor (OECT) biosensor for the detection of interleukin 6 (IL6), an important biomarker associated with various pathological processes, including chronic inflammation, inflammaging, cancer, and severe COVID-19 infection. The biosensor is functionalized with oligonucleotide aptamers engineered to bind specifically IL6. We developed an easy functionalization strategy based on gold nanoparticles deposited onto a poly(3,4-ethylenedioxythiophene) doped with polystyrenesulfonate (PEDOT:PSS) gate electrode for the subsequent electrodeposition of thiolated aptamers. During this functionalization step, the reduction of sulfide bonds allows for simultaneous deposition of a blocking agent. A detection range from picomolar to nanomolar concentrations for IL6 was achieved, and the selectivity of the device was assessed against Tumor Necrosis Factor (TNF), another cytokine involved in the inflammatory processes.

**KEYWORDS:** Interleukin-6, Cytokine, Organic electrochemical transistor, aptasensor, Aptamer, Biosensor



## INTRODUCTION

Cytokines are bioactive proteins involved in proinflammatory and anti-inflammatory processes. Environmental stimuli, stress or diseases may trigger the release of these proteins in a ripple effect for the activation of the immune system and/or various metabolic pathways.<sup>1,2</sup> Cytokine monitoring can thus be used to track progression of, e.g., infection, cancer, and acute or chronic inflammatory processes.<sup>3–5</sup> Interleukin-6 (IL6) is a low molecular weight glycoprotein that belongs to the family of cytokines. IL6 has multiple functions, since it can act both as an anti-inflammatory protein, inhibiting other cytokines release, or in pro-inflammatory processes, triggering the acute phase response of the innate immune system.<sup>6,7</sup> In physiological conditions and due to the local mode of action, IL6 is present in low concentrations (0.2–7.8 pg/mL; 10–300 fM)<sup>8</sup> in human serum. In contrast, IL6 concentrations are much higher in severe sepsis (1652 pg/mL; 60 pM) or septic shock (8518 pg/mL; 320 pM)<sup>9</sup> More recently, IL6 has also been associated with severe COVID-19 (SARS-CoV-2) infection. From preliminary studies, high levels (>3.5 pM)<sup>10</sup> of IL6 were correlated with respiratory failure and death, making this cytokine an important prognostic marker for the disease and pandemic progression.<sup>11</sup> For cytokine, in particular, IL6, detection and quantification represent a significant tool for precise monitoring of various diseases. Cytokines are present in fM-pM concentrations in bodily fluids; therefore, their detection requires both high sensitivity

and selectivity. State of the art quantification methods include enzyme-linked immunosorbent assays (ELISA, Supporting Information, Table S1) and antibody arrays. Although these methods are robust and standardized, they require bulky equipment and laborious protocols, characteristics that hinder their usage at the point of care or even in at-home settings.<sup>12</sup> For this reason, research has been focused on developing novel biosensor technologies for the rapid detection of these inflammatory biomarkers with miniaturized platform, such as electrochemical sensors<sup>13–16</sup> or field effect transistors (FETs, Supporting Information, Table 2).<sup>17–21</sup> Organic electrochemical transistors (OECTs) are now considered one of the most promising organic electronics technologies due to their high signal, low operation voltages, ease of fabrication, and ability to operate in aqueous environments.<sup>22,23</sup> OECTs are three terminal devices, where the gate electrode modulates the current in the channel (source–drain current,  $I_{SD}$ ) by inflow or outflow of cations from an electrolyte solution into the poly(3,4-ethylenedioxythiophene) doped with polystyrenesul-

**Special Issue:** Flexible Bioelectronics with a Focus on Europe

**Received:** August 20, 2023

**Revised:** November 29, 2023

**Accepted:** November 30, 2023

**Published:** December 23, 2023



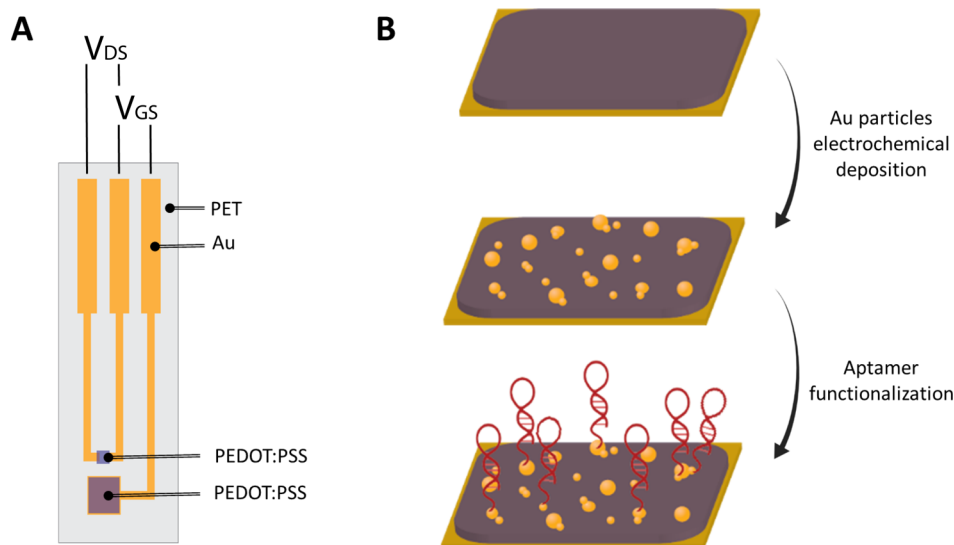


**Figure 1.** OEET-based aptasensor. (A) Schematic representation of the PEDOT:PSS based transistor planar configuration. Encapsulation (not shown) covers everything except the channel and the gate electrode.  $V_{DS}$  is the voltage between source and drain, and  $V_{GS}$  is the voltage applied between gate and source. (B) Gate functionalization steps: AuNP electrochemical deposition on PEDOT:PSS was followed by aptamer functionalization of the resulting composite.

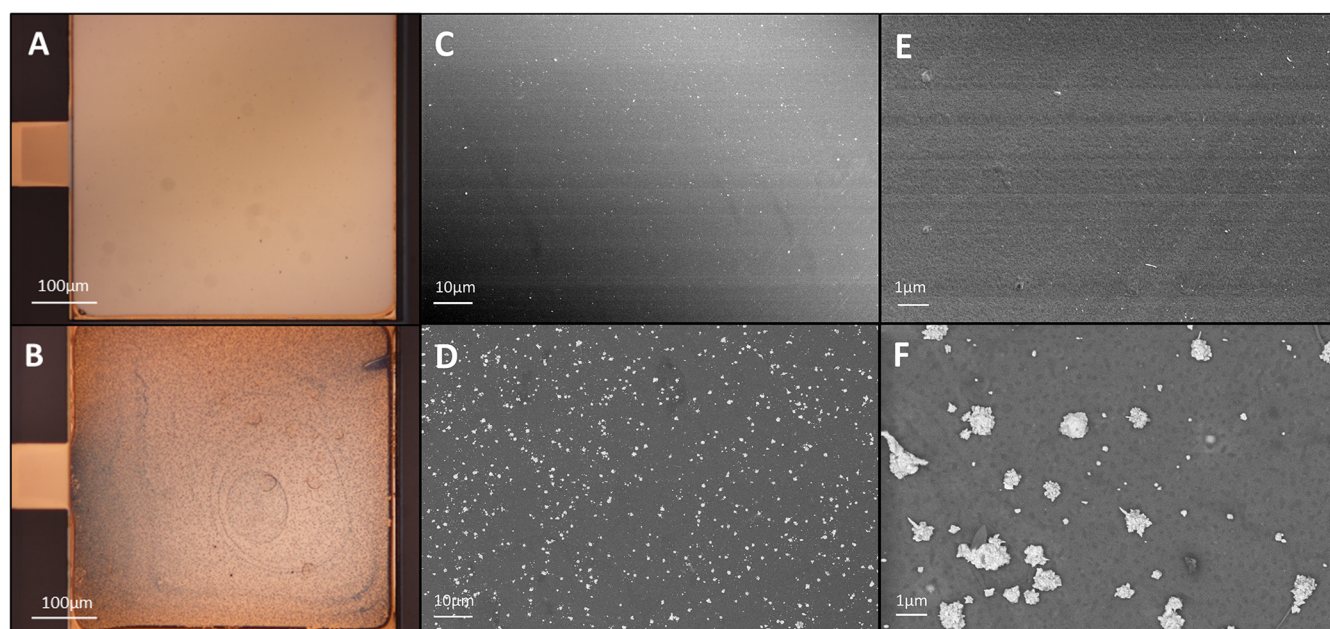


**Figure 2.** Modified gate electrode. Optical microscope images of the (A) PEDOT:PSS gate electrode and (B) AuNP/PEDOT:PSS. SEM images of (C, E) PEDOT:PSS and (D, F) the AuNP modified gate.

fonate (PEDOT:PSS) channel: small changes in gate voltage establish electrochemical modulation of the organic electronic channel, decreasing or increasing its conductivity, respectively.<sup>24,25</sup> Via appropriate functionalization, OEETs can selectively detect the metabolite of interest through changes in  $I_{SD}$ .<sup>22,26</sup> OEETs have been used as sensing platform for numerous analytes, exploiting the possibility of modulating  $I_{SD}$  either through faradaic reactions at the gate or via nonfaradaic mechanisms that rely purely on the permeability of the semiconducting channel to ions from the electrolyte. The detection mechanism is usually achieved through specific enzymatic reactions,<sup>27–35</sup> through molecularly imprinted polymers,<sup>36,37</sup> or using nonfaradaic antibody–antigen recognition.<sup>38–43</sup>

Although antibodies remain the gold standard sensing units (e.g., in ELISA), there is a growing interest in finding innovative, more reproducible and robust solutions, based on protein or oligonucleotide scaffolds.<sup>44</sup> Aptamers are oligonucleotide-based recognition elements which have been gaining interest due to their high selectivity, facility of synthesis, and low-cost development.<sup>45</sup> These probes are generated through a technique called Systematic Evolution of Ligand by Exponential Enrichment (SELEX), based on selection and amplification of oligonucleotide sequences which bind target molecules.<sup>46</sup> Aptamers were already employed successfully in electrochemical biosensors,<sup>47–50</sup> immunoassays,<sup>51–53</sup> and OEET-based biosensors.<sup>54–56</sup>

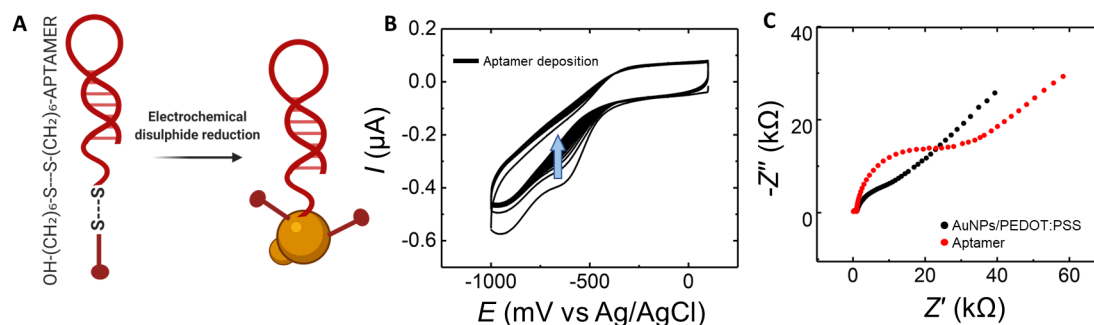


**Figure 3.** Aptamer functionalization. (A) Schematic representation of aptamer in solution and electrochemical disulfide reduction for AuNPs functionalization. (B) Cyclic voltammetry of AuNP/PEDOT:PSS gate electrode in 1  $\mu$ M aptamer solution from 0 V to  $-1$  V, 50 mV/s for 30 cycles. Trend indicated by arrow. (C) Impedance spectroscopy in ferricyanide 5 mM for AuNP/PEDOT:PSS electrode (black) and for the same electrode following aptamer immobilization (red).

In this work, we present a planar OECT-based biosensor for the label-free detection of IL6 via aptamer recognition. The successful integration of aptamers in the sensor is attained by means of an easy functionalization method using Au nanoparticle (AuNPs) deposition and electrochemical aptamer grafting on the organic electronic gate electrode surface, while examples with a removable gold wire as gate exist,<sup>17</sup> a planar geometry, and an easy functionalization strategy could aid in realizing a point-of-care device.

## RESULTS AND DISCUSSION

OECTs were fabricated on a poly(ethylene naphthalate) (PEN) foil with standard photolithographic techniques and presented the gate electrode and the channel in a planar configuration (Figure 1A). Gold source, drain, and gate electrodes delineated the transistor geometry, and a thin layer of PEDOT:PSS constituted the channel. An additional layer of PEDOT:PSS was deposited on the active area of the gate electrode to increase its capacitance and to better modulate the channel at low applied voltages (Figure 1A).

Conducting polymers and their composites have been widely used for analyte detection, even in cases in which they lack intrinsic specificity. Deposition of nanoparticles of different materials on polymer surfaces can provide additional physical-chemical properties, such as electrocatalytic activity using platinum nanoparticles (PtNPs) for peroxide detection<sup>27,34</sup> or an easier surface for functionalization, such as AuNPs for thiolate sensing units.<sup>57–60</sup> Here, the gate electrode was modified with AuNPs to provide a platform for aptamer binding. AuNP modification was performed via the electrochemical deposition of HAuCl<sub>4</sub> on the PEDOT:PSS film (Figure 1B). The optical microscope images in Figure 2 show the presence of the AuNPs/aggregates (Figure 2B) when compared to that of a bare PEDOT:PSS gate electrode (Figure 2A). Through scanning electron microscopy (SEM), it was possible to study the disposition and dimension of the Au particles, visible as dispersed aggregates with submicron dimensions. Figure 2D and 2E clearly demonstrate the presence of AuNPs on the surface, when compared to the bare PEDOT:PSS device in Figure 2C and 2E. The presence of gold on top of the PEDOT:PSS layer was further demonstrated through cyclic voltammetry with ferricyanide [Fe(CN)<sub>6</sub>]<sup>3–/4–</sup>. The bare PEDOT:PSS electrode did not show electrochemical redox peaks from ferricyanide, while the AuNP/PEDOT:PSS surface did show characteristic peaks (Figure S1A). In contrast with a planar bare gold gate

electrode with the same geometry, the PEDOT:PSS coated gate and AuNP/PEDOT:PSS showed better channel modulation, higher transconductance (Figure S1B), and faster transfer characteristic stabilization over time (Figure S1C).

The specific aptamer sequence selective for IL6 was developed by Rhinehardt et al, through SELEX, and evaluated with molecular dynamics analysis and Surface Plasmon Raman imaging (SPRI).<sup>61</sup> Furthermore, the sequence has already been proved applicable for IL6 biosensing technology based on Surface-Enhanced Raman Spectroscopy (SERS).<sup>62</sup> Functionalization of AuNPs with aptamer was performed via electrochemical disulfide reduction at the gate electrode. In solution, aptamers are present in their stabilized form, with the thiolate ending protected through a 6-mercapto-1-hexanol (MCH) residue (Figure 3A). MCH is a molecule often used in combination with aptamers to create an antifouling layer on the sensing surface.<sup>63,64</sup> We took advantage of the aptamer-MCH configuration, performing an electrochemical reduction at the gate electrode, binding both aptamer and linker to the gold particles. Figure 3B shows cyclic voltammetry of a AuNP/PEDOT:PSS gate electrode in an aptamer solution. We observed a decrease of cathodic current over time and the decrease of the reduction peak around  $-600$  mV vs Ag/AgCl, indicating the binding of aptamer and MCH to the electrode. To prove the presence of the aptamer on the AuNP/PEDOT:PSS surface, we performed faradaic electrochemical impedance spectroscopy (EIS) analysis on the gate electrode before and after aptamer deposition (Figure 3C). The binding of the aptamer and MCH to the AuNPs on the gate electrode created a barrier to the negatively charged redox molecule and consequently an increase in the charge transfer resistance (*R<sub>ct</sub>*), visible as a widening of the semicircular component of the trace toward larger *Z'*.

By using a fluorescent tag (Cy3) at the 3'-end of the sequence, we could obtain confocal fluorescent images of the functionalized gate (Figure 4). In Figure 4B, the fluorescent image of a fully functionalized gate with aptamers and a Cy3 tag is shown. Compared with a gate with only AuNP/PEDOT:PSS (Figure 4A), the gate area with fluorescent tagged oligonucleotides is evident. The control of fluorescent tagged aptamers on PEDOT:PSS without AuNP is shown in Figure 4C. While fluorescent spots are also visible without AuNP, the coverage is much lower. The functionalized gate surface was further studied using Fourier-transform infrared spectroscopy (FTIR) in attenuated total reflection (ATR) mode (Figure S2). FTIR-ATR confirms the presence of

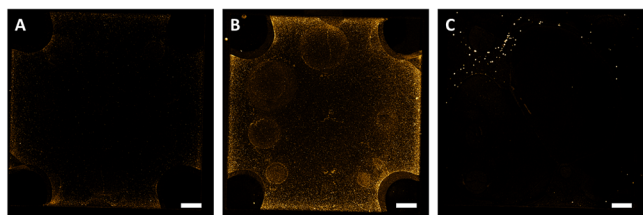


**Figure 4.** Fluorescent oligonucleotide functionalization. (A) Fluorescent image of AuNP/PEDOT:PSS (no Cy3-tag). (B) Fluorescence image with a Cy3 tag on the 3'-end (Cy3-aptamer/AuNP/PEDOT:PSS). (C) Cy3-aptamer on a gate without AuNP (Cy3-aptamer/PEDOT:PSS). Scale bar: 50  $\mu\text{m}$

oligonucleotides (aptamers) bound to the AuNP/PEDOT:PSS surface. The PEDOT:PSS peaks are stronger than the aptamer ones due to the greater abundance of the polymer compared to the DNA monolayer on the gold particles. In Figure S2 it is possible to notice visible changes from the AuNP/PEDOT:PSS surface (orange spectra) to the Aptamer/AuNP/PEDOT:PSS functionalized electrode (purple spectra). Specifically, there is an increase in absorption at  $1100\text{ cm}^{-1}$  (phosphate groups), along with weaker increases at  $1230\text{ cm}^{-1}$  (amine and phosphate groups) and  $1600\text{--}1700\text{ cm}^{-1}$  (amine and carbonyl groups). These changes in the spectra overlap in the absorption region with a reference electrode, which exhibits just bare gold and aptamer on the surface (violet spectra).

We monitored the OECT response for different concentrations of IL6, sweeping the voltage between source and gate ( $V_{\text{GS}}$ ) from 0.0 to 0.6 V and keeping the voltage between source and drain ( $V_{\text{DS}}$ ) fixed at  $-0.3\text{ V}$  (Figure 5A). The measurements were performed in phosphate buffer plus 0.05%

Tween-20 (polysorbate 20), containing increasing IL6 concentrations from 10 pM to 500 nM. Tween-20 is a surfactant commonly used in standard techniques like ELISA to reduce unspecific binding.<sup>65</sup> Here, we diluted the analyte of interest in solutions containing Tween-20 to prevent possible protein adsorption on either PEDOT:PSS or uncovered gold surfaces. Figure 5A shows an overlay of the transfer characteristics for increasing concentrations of IL6. The curves are characterized by the monotonic decrease of  $I_{\text{SD}}$  proportional to  $[\text{IL6}]$  when the gate is functionalized with aptamer. In order to quantify the response of the biosensor, we constructed the dose curve calculating the normalized response ( $NR$ ), for the IL6 analyte (Figure 5C) and for a control molecule TNF (Tumor Necrosis Factor), an analogous cytokine with different structure but similar function. Increasing concentrations of TNF induced much smaller current changes (Figure 5B) that, moreover, are not monotonic with  $[\text{IL6}]$  with  $NR_{I_{\text{SD}}}$  consistently around  $-0.1$  (inset Figure 5C). Similarly, an OECT without aptamer functionalization showed no monotonic behavior with  $[\text{IL6}]$  (Figure S3). Owing to the logarithmic variation of  $NR$  vs  $[\text{IL6}]$ , we immediately understand that the sensitivity of this device is greatly enhanced at the smallest concentrations, as  $dNR/dc$  scales as  $1/c$ , with  $c$  being the concentration. This sublinear response of our device is key to imparting a greater sensitivity at the lowest concentrations, which are the physio-pathological relevant in the case of IL6. A limit of detection (LOD) of about 24 pM was extracted as  $(m + 3\delta)$  using the TNF measurements as control solution (from four devices). In the formula,  $m$  is the average current value of the control solution and  $\delta$  its standard deviation.

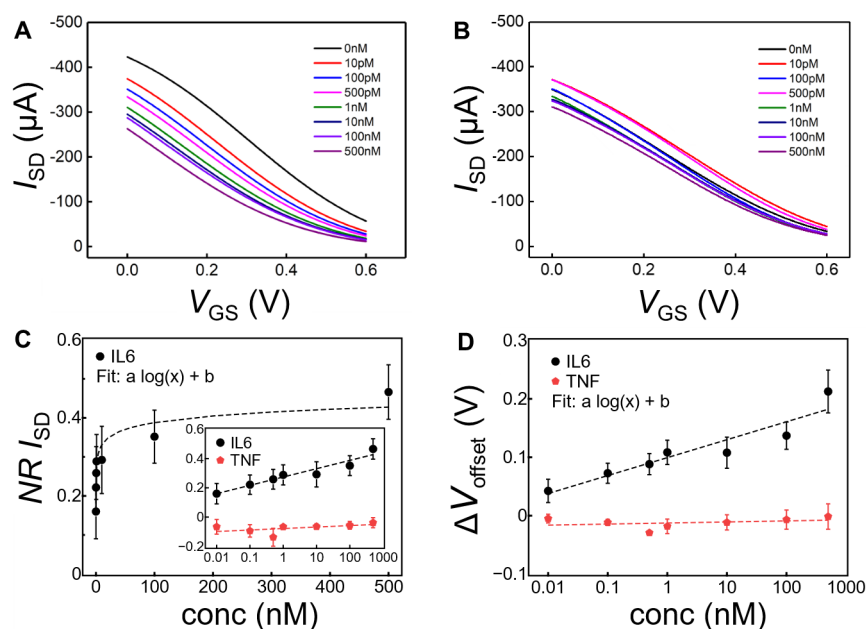


**Figure 5.** Interleukin-6 sensing. (A) Transfer characteristics of an OECT based aptasensor for increasing the concentration of IL6 in Tween buffer, recorded at fixed  $V_{\text{DS}}$   $-0.3\text{ V}$  and sweeping  $V_{\text{GS}}$  from 0 to 0.6 V. (B) Transfer characteristics of OECT based aptasensor for increasing concentration of TNF in Tween 20 buffer, recorded at fixed  $V_{\text{DS}}$   $-0.3\text{ V}$  and sweeping  $V_{\text{GS}}$  from 0 to 0.6 V. (C) Normalized response ( $NR_{I_{\text{SD}}}$ ) obtained for  $V_{\text{GS}}$  0.3 V upon increasing concentration of IL6 (black dots, fit:  $a = 2.5 \times 10^{-2}$  and  $b = 0.3$ ;  $n = 5$ ). The inset shows the lin/log graph with the dotted lines as an eye-guide with for IL6 (same as for lin/log plot), and for TNF (with parameters  $a = 4.4 \times 10^{-3}$  and  $b = -8 \times 10^{-2}$ ;  $n = 4$ ). (D) Gate voltage variations obtain for increasing concentration of IL6 (black dots, fit:  $a = 1.3 \times 10^{-2}$  and  $b = 0.1$ ;  $n = 5$ ) and TNF (red dots, fit:  $a = 8 \times 10^{-4}$  and  $b = -1.3 \times 10^{-2}$ ;  $n = 4$ ).

The working mechanism of p-type depletion mode OECT devices relies on the channel dedoping by cation inflow, accompanied by the ion migration from the electrolyte, upon application of increasing  $V_{GS}$ . The drain current  $I_{SD}$  depends on applied voltages and intrinsic material properties, and can be described following the model proposed by Bernardas and Malliaras:<sup>26</sup>

$$I_{SD}([IL6]) = \frac{Wt}{L} \frac{e\mu p_0}{V_p} \left( V_p - V_{GS}^{eff}([IL6]) + \frac{V_{DS}}{2} \right) V_{DS} \quad (1)$$

Here  $W$ ,  $t$ , and  $L$  are the channel width, thickness, and length,  $e$  is the elementary charge,  $\mu$  is the hole mobility in the channel,  $p_0$  is the initial hole density in the semiconductor,  $V_p$  is the pinchoff voltage, and  $V_{GS}^{eff}$  is the effective gate voltage. The latter depends on a voltage offset  $V_{offset}$  directly proportional to the concentration of the analyte when the gate electrode is functionalized with a specific biorecognition group, and the device is operated as a biosensor (Figure 5D):

$$V_{GS}^{eff} = V_{GS} + V_{offset}([IL6]) \quad (2)$$

The offset voltage represents a potential variation at gate/electrolyte interface,<sup>26,66</sup> induced by the binding between IL6 and aptamer, which consequently determines a current variation in the channel. As shown in Figure 5D, increasing concentration of IL6 produces an offset voltage variation (black dots, number of devices  $n = 5$ ), absent in the case of the control cytokine TNF (red dots,  $n = 4$ ). The corresponding logarithmic fit hints that the response is due to the contribution of the concentration to the potential drop at the gate/electrolyte interface. We further investigated the electrical characteristics, studying the changes in transconductance  $g_m$  (slope of the transfer curve) for increasing concentration of analytes (Figures S4A and S4B). We calculated the normalized response for the peak of  $g_m$  ( $NR_{g_m}$ ) (Figure S4C). Further we extracted the  $V_{GS}$  at which devices show the maximum transconductance, comparing the relative changes between 0 M and increasing analyte concentrations ( $NR_{V_{GS}}$ ). While the normalized response of  $g_m$  varied following both [IL6] and [TNF], implying that  $\Delta g_m$  may have a contribution from the device stress itself (Figure S4C), the normalized response for ( $V_{GS}$ ) at maximum transconductance is more selective toward IL6 concentrations (Figure S4D). The  $V_{GS}$  shows a decreasing behavior, upon increasing IL6 concentration, in contrast with the static TNF behavior. We hypothesized that this potential change ( $V_{GS}$ ) may be attributed to conformational aptamer adjustments upon IL6 binding, which could affect the charge density closer to the electrode surface, thus modifying the interface potential. EIS measurements for IL6 can be seen in Figure S5A. For comparison with the OECT sensor the highest normalized response was at 1 Hz and is compared to the OECT response in Figure S5B. It indicates that for concentrations lower than 100 nM the OECT sensor exhibits a higher response than EIS measurements.

## CONCLUSION

In this work, we showed an aptamer-based OECT biosensor for protein recognition. The sensor quantifies the concentration of the analyte of interest in pathological ranges against another analogous protein. The OECT shows changes in electrical characteristics such as  $I_{SD}$  current and  $V_{GS}$  for the maximum  $g_m$ , providing information on the binding between

aptamer and protein. Moreover, we show an easy functionalization strategy based on electrochemical AuNP deposition and electrochemical reduction of the sensing unit at the gate electrode. This electrochemical reduction step of the sensing unit allows for not only targeted deposition on the aptamer but also a simultaneous deposition of a blocking agent, further simplifying the fabrication process. In particular, when envisioning a portable sensing platform to detect multiple analytes, this strategy is advantageous compared to chemically reducing the thiol bond of the sensing unit. These strategies, together with the fabrication steps, make the device disposable and functional for a point of care application, paving the way for easy health monitoring. Further advancement will foresee integration with microfluidics and multiple detection of cytokines on different OECT, to allow a more complete understanding of the inflammatory condition of the patient.

## MATERIALS AND METHODS

**Device Fabrication.** A circular 4 in. substrate was obtained by cutting poly(ethylene naphthalate) (PEN) foil (Teonex Q65HA, 125  $\mu\text{m}$ , Peutz Folien GmbH). After the PEN foil was cleaned with water and acetone, 2 nm chromium (Cr) and 50 nm gold (Au) were thermally evaporated onto the surface. Gold contacts, wirings and gates were patterned using a Shipley 1805 positive resist and photolithography (Karl Suss MA/BM 6 mask aligner), then wet etched in  $\text{I}_2/\text{KI}$  solution for Au, and  $\text{H}_2\text{O}_2/\text{NH}_4\text{Cl}/\text{H}_2\text{O}$  for Cr. The substrate was then stripped with acetone. Channels and gates were deposited by spin coating (1400 rpm for 30s) with a PEDOT:PSS (Clevios PH1000) solution with 5% v/v ethylene glycol and 1% v/v GOPS (3-glycidyloxypropyl)trimethoxysilane) and dodecylbenzenesulfonic acid (1 drop per 5 mL) and patterned using a Shipley 1813 positive resist, after baking at 120  $^\circ\text{C}$  for 2h. The substrate was then dry reactive ion etched with  $\text{CF}_4/\text{O}_2$  and stripped with acetone. The channel has a geometry of 20  $\mu\text{m} \times 100 \mu\text{m}$  and the gate of 250  $\mu\text{m} \times 250 \mu\text{m}$ . As a final step, the substrate was encapsulated with SU-8 2010 (MicroChem) and openings were defined by using wet etching with developer mr-Dev 600 (Microresist Technology). Chemicals were used as received from Sigma-Aldrich unless stated otherwise.

**Gate Functionalization.** Gold nanoparticles were formed by applying  $-0.273$  V vs Ag/AgCl in 3 mM HAuCl<sub>4</sub> in 0.1 M KCl for 60 s through electrochemical deposition (CH Instruments potentiostat 760c model with a three-electrode setup) at the gate electrode. Devices were then rinsed thoroughly with DI water. The aptamer sequence (5'-CTT CCA ACG CTC GTA TTG TCA GTC TTT AGT-3') was found in the literature.<sup>61</sup> This sequence, with a thiolated 6-mercapto-1-hexanol group (MCH) at the 5' end, was purchased from Sigma-Aldrich. A solution of 1  $\mu\text{M}$  aptamer in 10 mM phosphate buffered saline (PBS) was used for electrochemical deposition of the oligomer on the gold particles, using cyclic voltammetry for 30 cycles from 0.1 to  $-1$  V at 50 mV/s on the gate electrode. After DI water rinsing, the surface electrode was rearranged in a solution of KCl 50 mM for 20 cycles from  $-0.1$  to 0.1 V at 50 mV/s. The active area of the device was then incubated in 0.05% Tween 20 buffer in 10 mM PBS for 1 h. Gold nanoparticle deposition was observed performing cyclic voltammetry in 5 mM ferricyanide solution at the gate electrode from  $-0.5$  to 0.5 V at 50 mV/s for 2 cycles. AuNP deposition was also studied with optical and scanning electron microscopy (SEM). Aptamer deposition was observed through impedance measurements in 5 mM ferricyanide and with Fourier-transform infrared spectroscopy in attenuated total reflectance mode (FTIR-ATR) by using a Bruker Equinox 55 spectrometer equipped with a Bruker Platinum ATR single reflection accessory. The spectra were accumulated over 50 scans in the range 4000 to 500  $\text{cm}^{-1}$  with a resolution of 4  $\text{cm}^{-1}$  using a zero-filling factor of 2. The background measurement was PEN with a thermally evaporated Au layer, like the substrate used for device preparation. (Additional corrections, such as baseline adjustments, have not been applied to the measured data.) Fluorescent microscopy images were taken with a Zeiss LSM 980, Airyscan 2

(Carl Zeiss AG). The sequence for the fluorescent image was 5'-ThioMC6-D/AAA AAA TTA CCG GGC TCT GCC ATC T/3Cy-3' with a thiol group at the 5' end and a Cy3-tag at the 3' end.

**Electrical Characterization.** Electrical measurements were performed in 10 mM PBS buffer with or without 0.05% Tween 20. Buffer with Tween 20 was used in experiments for sensing IL-6. Source, gate, and drain electrodes were connected to a Keithley 2600 source meter, and all measurements were carried out at room temperature. The transfer characteristics were performed by keeping the voltage between source and drain fixed at  $V_{DS} = -0.3$  V and sweeping the voltage between source and gate  $V_{GS}$  from 0 to 0.6 V. The OECT was incubated with increasing concentration of IL6 or TNF in Tween 20 buffer for 15 min and then recorded until current stabilization (no variation in the CV noticeable anymore, approximately 10 min). Au, PEDOT:PSS, and AuNP/PEDOT:PSS electrodes were stabilized by sweeping gate voltage from 0 to 0.6 V and keeping the source–drain voltage fixed at  $-0.3$  V for 15 min.

**Data Analysis.** To quantify and compare different devices, a normalized  $I_{SD}$  response ( $NR_{I_{SD}}$ ) was defined as

$$NR_{I_{SD}} = -\frac{I_n - I_0}{I_0} \quad (3)$$

where  $I_n$  is the current taken at  $V_{GS} = 0.3$  V for each  $n^{\text{th}}$  concentration of IL6 and TNF, and  $I_0$  is the baseline current at  $V_{GS} = 0.3$  V for the solution at 0 M analyte concentration. The normalized  $g_m$  response was similarly calculated as

$$NR_{g_m}([\text{IL6}]) = \frac{g_m([\text{IL6}]) - g_{m,0}}{g_{m,0}} \quad (4)$$

where  $g_m([\text{IL6}])$  is the transconductance peak value at concentration  $[\text{IL6}]$  (and similarly for TNF) and  $g_{m,0}$  is the transconductance for the solution at 0 M analyte concentration. The sensor's capability was also investigated by comparing relative changes at the  $V_{GS}$  for the maximum  $g_m$  using

$$NR_{V_{GS}} = \frac{(V_{GS,n} - V_{GS,0})}{V_{GS,0}} \quad (5)$$

where  $V_{GS}([\text{IL6}])$  is the voltage between gate and source for maximum  $g_m$  taken for each concentration of IL6 (and similarly with TNF) and  $V_{GS,0}$  is the voltage between source and gate for maximum  $g_m$  for the solution at 0 M analyte concentration.

## ■ ASSOCIATED CONTENT

### Data Availability Statement

Experimental data are available on Zenodo.<sup>67</sup>

### SI Supporting Information

The Supporting Information is available free of charge at <https://pubs.acs.org/doi/10.1021/acsami.3c12397>.

Table S1, ELISA kits for IL-6 detection; Table S2, cytokine sensors with electrolyte gated organic transistors; Figure S1, AuNP/PEDOT:PSS electrical characteristics; Figure S2, FTIR-ATR measurements; Figure S3, IL6 detection on AuNP/PEDOT:PSS gate; Figure S4, transconductance of OECT based aptasensor; and Figure S5, comparison of OECT and electrochemical impedance spectroscopy sensor responses (PDF)

## ■ AUTHOR INFORMATION

### Corresponding Authors

**Daniel T. Simon** – *Laboratory of Organic Electronics, Department of Science and Technology, Linköping University, 601 74 Norrköping, Sweden*; [orcid.org/0000-0002-2799-3490](https://orcid.org/0000-0002-2799-3490); Email: [daniel.simon@liu.se](mailto:daniel.simon@liu.se)

**Carlo A. Bortolotti** – *Dipartimento di Scienze della Vita, Università di Modena e Reggio Emilia, 41125 Modena, Italy*; [orcid.org/0000-0002-5701-5727](https://orcid.org/0000-0002-5701-5727); Email: [carloaugusto.bortolotti@unimore.it](mailto:carloaugusto.bortolotti@unimore.it)

## Authors

**Chiara Diacci** – *Laboratory of Organic Electronics, Department of Science and Technology, Linköping University, 601 74 Norrköping, Sweden*; *Dipartimento di Scienze della Vita, Università di Modena e Reggio Emilia, 41125 Modena, Italy*

**Bernhard Burtscher** – *Laboratory of Organic Electronics, Department of Science and Technology, Linköping University, 601 74 Norrköping, Sweden*

**Marcello Berto** – *Dipartimento di Scienze della Vita, Università di Modena e Reggio Emilia, 41125 Modena, Italy*; [orcid.org/0000-0002-3356-8829](https://orcid.org/0000-0002-3356-8829)

**Tero-Petri Ruoko** – *Laboratory of Organic Electronics, Department of Science and Technology, Linköping University, 601 74 Norrköping, Sweden*; Present Address: Faculty of Engineering and Natural Sciences, Tampere University, 33101 Tampere, Finland

**Samuel Lienemann** – *Laboratory of Organic Electronics, Department of Science and Technology, Linköping University, 601 74 Norrköping, Sweden*

**Pierpaolo Greco** – *Department of Neuroscience and Rehabilitation, Università di Ferrara, 44121 Ferrara, Italy*; *Center for Translational Neurophysiology of Speech and Communication, Istituto Italiano di Tecnologia, 44100 Ferrara, Italy*

**Magnus Berggren** – *Laboratory of Organic Electronics, Department of Science and Technology, Linköping University, 601 74 Norrköping, Sweden*; [orcid.org/0000-0001-5154-0291](https://orcid.org/0000-0001-5154-0291)

**Marco Borsari** – *Dipartimento di Scienze Chimiche e Geologiche, Università di Modena e Reggio Emilia, 41125 Modena, Italy*; [orcid.org/0000-0002-3612-4764](https://orcid.org/0000-0002-3612-4764)

**Fabio Biscarini** – *Dipartimento di Scienze della Vita, Università di Modena e Reggio Emilia, 41125 Modena, Italy*; *Center for Translational Neurophysiology of Speech and Communication, Istituto Italiano di Tecnologia, 44100 Ferrara, Italy*; [orcid.org/0000-0001-6648-5803](https://orcid.org/0000-0001-6648-5803)

Complete contact information is available at:

<https://pubs.acs.org/10.1021/acsami.3c12397>

## Notes

The authors declare no competing financial interest.

## ■ ACKNOWLEDGMENTS

This project has received funding from the European Union's Horizon 2020 research and innovation programme under Marie Skłodowska-Curie Grant Agreement No. 813863. Additional support was provided by the Knut and Alice Wallenberg Foundation, the Swedish Foundation for Strategic Research, and the Swedish Research Council.

## ■ REFERENCES

- (1) Holloway, A. F.; Rao, S.; Shannon, M. F. Regulation of Cytokine Gene Transcription in the Immune System. *Mol. Immunol.* **2002**, *38* (8), 567–580.
- (2) Spurlock, M. E. Regulation of Metabolism and Growth during Immune Challenge: An Overview of Cytokine Function. *J. Anim. Sci.* **1997**, *75* (7), 1773–1783.

- (3) Gabay, C. Interleukin-6 and Chronic Inflammation. *Arthritis Res. Ther.* **2006**, *8* (2), S3.
- (4) Velazquez-Salinas, L.; Verdugo-Rodriguez, A.; Rodriguez, L. L.; Borca, M. V. The Role of Interleukin 6 During Viral Infections. *Frontiers in Microbiology* **2019**, *10*, 1057.
- (5) Kumari, N.; Dwarakanath, B. S.; Das, A.; Bhatt, A. N. Role of Interleukin-6 in Cancer Progression and Therapeutic Resistance. *Tumor Biol.* **2016**, *37* (9), 11553–11572.
- (6) Nishimoto, N.; Kishimoto, T. Interleukin 6: From Bench to Bedside. *Nat. Clin. Pract. Rheumatol.* **2006**, *2* (11), 619–626.
- (7) Tanaka, T.; Narazaki, M.; Kishimoto, T. IL-6 in Inflammation, Immunity, and Disease. *Cold Spring Harbor Perspectives in Biology* **2014**, *6* (10), a016295.
- (8) Molano Franco, D.; Arevalo-Rodriguez, I.; Roqué i Figuls, M.; Zamora, J. Interleukin-6 for Diagnosis of Sepsis in Critically Ill Adult Patients. *Cochrane Database Syst. Rev.* **2015**, *2015* (7), No. CD011811.
- (9) Damas, P.; Canivet, J.-L.; De Groote, D.; Vrindts, Y.; Albert, A.; Franchimont, P.; Lamy, M. Sepsis and Serum Cytokine Concentrations. *Crit. Care Med.* **1997**, *25* (3), 405.
- (10) Herold, T.; Jurinovic, V.; Arnreich, C.; Hellmuth, J. C.; von Bergwelt-Baildon, M.; Klein, M.; Weinberger, T. Level of IL-6 Predicts Respiratory Failure in Hospitalized Symptomatic COVID-19 Patients. *medRxiv* 2020; DOI: 10.1101/2020.04.01.20047381.
- (11) Coomes, E. A.; Haghbayan, H. Interleukin-6 in Covid-19: A Systematic Review and Meta-Analysis. *Rev. Med. Virol.* **2020**, *30* (6), No. 1.
- (12) Liu, G.; Qi, M.; Hutchinson, M. R.; Yang, G.; Goldys, E. M. Recent Advances in Cytokine Detection by Immunosensing. *Biosens. Bioelectron.* **2016**, *79*, 810.
- (13) Loo, S. W.; Pui, T.-S. Cytokine and Cancer Biomarkers Detection: The Dawn of Electrochemical Paper-Based Biosensor. *Sensors.* **2020**, *20*, 1854.
- (14) Russell, C.; Ward, A. C.; Vezza, V.; Hoskisson, P.; Alcorn, D.; Stenson, D. P.; Corrigan, D. K. Development of a Needle Shaped Microelectrode for Electrochemical Detection of the Sepsis Biomarker Interleukin-6 (IL-6) in Real Time. *Biosens. Bioelectron.* **2019**, *126*, 806.
- (15) Aydın, E. B.; Sezgintürk, M. K. An Impedimetric Immunosensor for Highly Sensitive Detection of IL-8 in Human Serum and Saliva Samples: A New Surface Modification Method by 6-Phosphonohexanoic Acid for Biosensing Applications. *Anal. Biochem.* **2018**, *554*, 44.
- (16) Filik, H.; Avan, A. A. Electrochemical Immunosensors for the Detection of Cytokine Tumor Necrosis Factor Alpha: A Review. *Talanta* **2020**, *211*, No. 120758.
- (17) Diacci, C.; Berto, M.; Di Lauro, M.; Bianchini, E.; Pinti, M.; Simon, D. T.; Biscarini, F.; Bortolotti, C. A. Label-Free Detection of Interleukin-6 Using Electrolyte Gated Organic Field Effect Transistors. *Biointerphases* **2017**, *12* (5), No. 05F401.
- (18) Berto, M.; Diacci, C.; D'Agata, R.; Pinti, M.; Bianchini, E.; Lauro, M. Di; Casalini, S.; Cossarizza, A.; Berggren, M.; Simon, D.; Spoto, G.; Biscarini, F.; Bortolotti, C. A. EGOFET Peptide Aptasensor for Label-Free Detection of Inflammatory Cytokines in Complex Fluids. *Adv. Biosyst.* **2018**, *2* (2), 1–8.
- (19) Berto, M.; Casalini, S.; Di Lauro, M.; Marasso, S. L.; Cocuzza, M.; Perrone, D.; Pinti, M.; Cossarizza, A.; Pirri, C. F.; Simon, D. T.; Berggren, M.; Zerbetto, F.; Bortolotti, C. A.; Biscarini, F. Biorecognition in Organic Field Effect Transistors Biosensors: The Role of the Density of States of the Organic Semiconductor. *Anal. Chem.* **2016**, *88* (24), 12330–12338.
- (20) Parkula, V.; Berto, M.; Diacci, C.; Patraha, B.; Di Lauro, M.; Kovtun, A.; Liscio, A.; Sensi, M.; Samori, P.; Greco, P.; Bortolotti, C. A.; Biscarini, F. Harnessing Selectivity and Sensitivity in Electronic Biosensing: A Novel Lab-on-Chip Multigate Organic Transistor. *Anal. Chem.* **2020**, *92* (13), 9330–9337.
- (21) Khan, N. I.; Song, E. Detection of an IL-6 Biomarker Using a GFET Platform Developed with a Facile Organic Solvent-Free Aptamer Immobilization Approach. *Sensors* **2021**, *21* (4), 1335.
- (22) Strakosas, X.; Bongo, M.; Owens, R. M. The Organic Electrochemical Transistor for Biological Applications. *J. Appl. Polym. Sci.* **2015**, *132* (15), 1–14.
- (23) Malliaras, G. G.; Berggren, M.; Owens, R. M.; Rivnay, J.; Inal, S.; Salleo, A. Organic Electrochemical Transistors. *Nat. Rev. Mater.* **2018**, *3* (2), No. 17086.
- (24) Bernards, D. A.; Malliaras, G. G. Steady-State and Transient Behavior of Organic Electrochemical Transistors. *Adv. Funct. Mater.* **2007**, *17* (17), 3538–3544.
- (25) Nissa, J.; Janson, P.; Simon, D. T.; Berggren, M. Expanding the Understanding of Organic Electrochemical Transistor Function. *Appl. Phys. Lett.* **2021**, *118* (5), No. 053301.
- (26) Bernards, D. A.; MacAya, D. J.; Nikolou, M.; Defranco, J. A.; Takamatsu, S.; Malliaras, G. G. Enzymatic Sensing with Organic Electrochemical Transistors. *J. Mater. Chem.* **2008**, *18* (1), 116–120.
- (27) Diacci, C.; Abedi, T.; Lee, J. W.; Gabrielson, E. O.; Berggren, M.; Simon, D. T.; Niittylä, T.; Stavrinidou, E. Diurnal in Vivo Xylem Sap Glucose and Sucrose Monitoring Using Implantable Organic Electrochemical Transistor Sensors. *iScience* **2021**, *24* (1), 101966.
- (28) Diacci, C.; Lee, J. W.; Janson, P.; Dufil, G.; Méhes, G.; Berggren, M.; Simon, D. T.; Stavrinidou, E. Real-Time Monitoring of Glucose Export from Isolated Chloroplasts Using an Organic Electrochemical Transistor. *Adv. Mater. Technol.* **2020**, *5* (3), 1900262.
- (29) Galliani, M.; Diacci, C.; Berto, M.; Sensi, M.; Beni, V.; Berggren, M.; Borsari, M.; Simon, D. T.; Biscarini, F.; Bortolotti, C. A. Flexible Printed Organic Electrochemical Transistors for the Detection of Uric Acid in Artificial Wound Exudate. *Adv. Mater. Interfaces* **2020**, DOI: 10.1002/admi.202001218.
- (30) Pappa, A. M.; Curto, V. F.; Braendlein, M.; Strakosas, X.; Donahue, M. J.; Fiocchi, M.; Malliaras, G. G.; Owens, R. M. Organic Transistor Arrays Integrated with Finger-Powered Microfluidics for Multianalyte Saliva Testing. *Adv. Healthc. Mater.* **2016**, *5* (17), 2295–2302.
- (31) Khodagholy, D.; Curto, V. F.; Fraser, K. J.; Gurfinkel, M.; Byrne, R.; Diamond, D.; Malliaras, G. G.; Benito-Lopez, F.; Owens, R. M. Organic Electrochemical Transistor Incorporating an Ionogel as a Solid State Electrolyte for Lactate Sensing. *J. Mater. Chem.* **2012**, *22* (10), 4440–4443.
- (32) Kergoat, L.; Piro, B.; Simon, D. T.; Pham, M. C.; Noël, V.; Berggren, M. Detection of Glutamate and Acetylcholine with Organic Electrochemical Transistors Based on Conducting Polymer/Platinum Nanoparticle Composites. *Adv. Mater.* **2014**, *26* (32), 5658–5664.
- (33) Scheiblin, G.; Aliane, A.; Strakosas, X.; Curto, V. F.; Coppard, R.; Marchand, G.; Owens, R. M.; Mailley, P.; Malliaras, G. G. Screen-Printed Organic Electrochemical Transistors for Metabolite Sensing. *MRS Commun.* **2015**, *5* (3), S07–S11.
- (34) Strakosas, X.; Huerta, M.; Donahue, M. J.; Hama, A.; Pappa, A.-M.; Ferro, M.; Ramuz, M.; Rivnay, J.; Owens, R. M. Catalytically Enhanced Organic Transistors for in Vitro Toxicology Monitoring through Hydrogel Entrapment of Enzymes. *J. Appl. Polym. Sci.* **2017**, *134* (7), 519.
- (35) Pappa, A. M.; Ohayon, D.; Giovannitti, A.; Maria, I. P.; Savva, A.; Uguz, I.; Rivnay, J.; McCulloch, I.; Owens, R. M.; Inal, S. Direct Metabolite Detection with an N-Type Accumulation Mode Organic Electrochemical Transistor. *Sci. Adv.* **2018**, *4* (6), 1–8.
- (36) Zhang, L.; Liu, Z.; Xiong, C.; Zheng, L.; Ding, Y.; Lu, H.; Zhang, G.; Qiu, L. Selective Recognition of Histidine Enantiomers Using Novel Molecularly Imprinted Organic Transistor Sensor. *Org. Electron.* **2018**, *61* (March), 254–260.
- (37) Parlak, O.; Keene, S. T.; Marais, A.; Curto, V. F.; Salleo, A. Molecularly Selective Nanoporous Membrane-Based Wearable Organic Electrochemical Device for Noninvasive Cortisol Sensing. *Sci. Adv.* **2018**, *4* (7), eaar2904.
- (38) Gentili, D.; D'Angelo, P.; Militano, F.; Mazzei, R.; Poerio, T.; Bruciale, M.; Tarabella, G.; Bonetti, S.; Marasso, S. L.; Cocuzza, M.; Giorno, L.; Iannotta, S.; Cavallini, M. Integration of Organic Electrochemical Transistors and Immuno-Affinity Membranes for Label-Free Detection of Interleukin-6 in the Physiological Concen-

- tration Range through Antibody-Antigen Recognition. *J. Mater. Chem. B* **2018**, *6* (33), 5400–5406.
- (39) Macchia, E.; Ghittorelli, M.; Torricelli, F.; Torsi, L. Organic Electrochemical Transistor Immuno-Sensor Operating at the Femtomolar Limit of Detection. *Proc. - 2017 7th Int. Work. Adv. Sensors Interfaces, IWASI 2017* **2017**, 68–72.
- (40) Decataldo, F.; Druet, V.; Pappa, A. M.; Tan, E.; Savva, A.; Pitsalidis, C.; Inal, S.; Kim, J. S.; Fraboni, B.; Owens, R. M.; Iandolo, D. BMP-2 Functionalized PEDOT:PSS-Based OECTs for Stem Cell Osteogenic Differentiation Monitoring. *Flex. Print. Electron.* **2019**, *4* (4), 044006.
- (41) Guo, K.; Wustoni, S.; Koklu, A.; Diaz-galicia, E.; Mcculloch, I.; Arold, S. T.; Grünberg, R.; Inal, S. A Nanobody-Functionalized Organic Electrochemical Transistor for the Rapid Detection of SARS-CoV-2 and MERS Antigens at the Physical Limit. *medRxiv* **2020**; .
- (42) Yu, J.; Yang, A.; Wang, N.; Ling, H.; Song, J.; Chen, X.; Lian, Y.; Zhang, Z.; Yan, F.; Gu, M. Highly Sensitive Detection of Caspase-3 Activity Based on Peptide-Modified Organic Electrochemical Transistor Biosensors. *Nanoscale* **2021**, *13* (5), 2868–2874.
- (43) Manco Urbina, P. A.; Berto, M.; Greco, P.; Sensi, M.; Borghi, S.; Borsari, M.; Bortolotti, C. A.; Biscarini, F. Physical Insights from the Frumkin Isotherm Applied to Electrolyte Gated Organic Transistors as Protein Biosensors. *J. Mater. Chem. C* **2021**, *9* (33), 10965–10974.
- (44) Löfblom, J.; Frejd, F. Y.; Ståhl, S. Non-Immunoglobulin Based Protein Scaffolds. *Curr. Opin. Biotechnol.* **2011**, *22* (6), 843–848.
- (45) Adachi, T.; Nakamura, Y. Aptamers: A Review of Their Chemical Properties and Modifications for Therapeutic Application. *Molecules* **2019**, *24* (23), 4229.
- (46) Zhuo, Z.; Yu, Y.; Wang, M.; Li, J.; Zhang, Z.; Liu, J.; Wu, X.; Lu, A.; Zhang, G.; Zhang, B. Recent Advances in SELEX Technology and Aptamer Applications in Biomedicine. *International Journal of Molecular Sciences* **2017**, *18*, 2142.
- (47) Feng, L.; Chen, Y.; Ren, J.; Qu, X. A Graphene Functionalized Electrochemical Aptasensor for Selective Label-Free Detection of Cancer Cells. *Biomaterials* **2011**, *32* (11), 2930–2937.
- (48) Zhang, Y.-L.; Huang, Y.; Jiang, J.-H.; Shen, G.-L.; Yu, R.-Q. Electrochemical Aptasensor Based on Proximity-Dependent Surface Hybridization Assay for Single-Step, Reusable, Sensitive Protein Detection. *J. Am. Chem. Soc.* **2007**, *129* (50), 15448–15449.
- (49) Jolly, P.; Miodek, A.; Yang, D.; Chen, L.; Lloyd, M. D.; Estrela, P. Electro-Engineered Polymeric Films for the Development of Sensitive Aptasensors for Prostate Cancer Marker Detection. *ACS Sens.* **2016**, *1*, 1308–1314.
- (50) Kumar, L. S. S.; Wang, X.; Hagen, J.; Naik, R.; Papautsky, I.; Heikenfeld, J. Label Free Nano-Aptasensor for Interleukin-6 in Protein-Dilute Bio Fluids Such as Sweat. *Anal. Methods* **2016**, *8* (17), 3440–3444.
- (51) Toh, S. Y.; Citartan, M.; Gopinath, S. C. B.; Tang, T.-H. Aptamers as a Replacement for Antibodies in Enzyme-Linked Immunosorbent Assay. *Biosens. Bioelectron.* **2015**, *64*, 392–403.
- (52) Ferreira, C. S. M.; Papamichael, K.; Guilbault, G.; Schwarzacher, T.; Garipey, J.; Missailidis, S. DNA Aptamers against the MUC1 Tumour Marker: Design of Aptamer–Antibody Sandwich ELISA for the Early Diagnosis of Epithelial Tumours. *Anal. Bioanal. Chem.* **2008**, *390* (4), 1039–1050.
- (53) Wang, J.; Lv, R.; Xu, J.; Xu, D.; Chen, H. Characterizing the Interaction between Aptamers and Human IgE by Use of Surface Plasmon Resonance. *Anal. Bioanal. Chem.* **2008**, *390* (4), 1059–1065.
- (54) Liang, Y.; Guo, T.; Zhou, L.; Offenhäusser, A.; Mayer, D. Label-Free Split Aptamer Sensor for Femtomolar Detection of Dopamine by Means of Flexible Organic Electrochemical Transistors. *Mater. (Basel, Switzerland)* **2020**, *13* (11), 2577.
- (55) Liang, Y.; Wu, C.; Figueroa-Miranda, G.; Offenhäusser, A.; Mayer, D. Amplification of Aptamer Sensor Signals by Four Orders of Magnitude via Interdigitated Organic Electrochemical Transistors. *Biosens. Bioelectron.* **2019**, *144*, No. 111668.
- (56) Prabhakar, P.; Sen, R. K.; Dwivedi, N.; Khan, R.; Solanki, P. R.; Srivastava, A. K.; Dhand, C. 3D-Printed Microfluidics and Potential Biomedical Applications. *Front. Nanotechnol.* **2021**, *3*, 6.
- (57) Spain, E.; Keyes, T. E.; Forster, R. J. DNA Sensor Based on Vapour Polymerised Pedot Films Functionalised with Gold Nanoparticles. *Biosens. Bioelectron.* **2013**, *41* (1), 65–70.
- (58) Gu, Y.; Tseng, P.-Y.; Bi, X.; Yang, J. H. C. Quantification of DNA by a Thermal-Durable Biosensor Modified with Conductive Poly(3,4-Ethylenedioxythiophene). *Sensors (Basel)* **2018**, *18* (11), 3684.
- (59) Su, W.; Cho, M.; Nam, J.-D.; Choe, W.-S.; Lee, Y. Aptamer-Assisted Gold Nanoparticles/PEDOT Platform for Ultrasensitive Detection of LPS. *Electroanalysis* **2013**, *25* (2), 380–386.
- (60) Kim, M.; Iezzi, R.; Shim, B. S.; Martin, D. C. Impedimetric Biosensors for Detecting Vascular Endothelial Growth Factor (VEGF) Based on Poly(3,4-Ethylene Dioxothiophene) (PEDOT)/Gold Nanoparticle (Au NP) Composites. *Front. Chem.* **2019**, *7* (MAR), 1–11.
- (61) Rhinehardt, K. L.; Vance, S. A.; Mohan, R. V.; Sandros, M.; Srinivas, G. Molecular Modeling and SPRI Investigations of Interleukin (IL6) Protein and DNA Aptamers. *J. Biomol. Struct. Dyn.* **2018**, *36* (8), 1934–1947.
- (62) Muhammad, M.; Shao, C.; Huang, Q. Aptamer-Functionalized Au Nanoparticles Array as the Effective SERS Biosensor for Label-Free Detection of Interleukin-6 in Serum. *Sensors Actuators B Chem.* **2021**, *334*, No. 129607.
- (63) Miodek, A.; Regan, E. M.; Bhalla, N.; Hopkins, N. A. E.; Goodchild, S. A.; Estrela, P. Optimisation and Characterisation of Anti-Fouling Ternary SAM Layers for Impedance-Based Aptasensors. *Sensors (Switzerland)* **2015**, *15* (10), 25015–25032.
- (64) Aliakbarinodehi, N.; Jolly, P.; Bhalla, N.; Miodek, A.; De Micheli, G.; Estrela, P.; Carrara, S. Aptamer-Based Field-Effect Biosensor for Tenofovir Detection. *Sci. Rep.* **2017**, *7* (1), No. 44409.
- (65) Steinitz, M. Quantitation of the Blocking Effect of Tween 20 and Bovine Serum Albumin in ELISA Microwells. *Anal. Biochem.* **2000**, *282* (2), 232–238.
- (66) Nakatsuka, N.; Yang, K.-A.; Abendroth, J. M.; Cheung, K. M.; Xu, X.; Yang, H.; Zhao, C.; Zhu, B.; Rim, Y. S.; Yang, Y.; Weiss, P. S.; Stojanović, M. N.; Andrews, A. M. Aptamer–Field-Effect Transistors Overcome Debye Length Limitations for Small-Molecule Sensing. *Science (80-)* **2018**, *362* (6412), 319–324.
- (67) Organic Electrochemical Transistor Aptasensor for Interleukin-6 Detection; Data. DOI: 10.5281/zenodo.10053241.